energies

MDPI

Article

Origin and Biodegradation of Crude Oils from the Northernmost Fields in the Bolivar Coastal Complex (Zulia State, Venezuela)

Marcos Escobar [1], Gonzalo Márquez [2], Blanca Guerrero [3], Patricia Marín [2], Carlos Boente [2,*], Antonio Bernardo-Sánchez [4], Emilio Romero [2] and Albert Permanyer [5]

1 Postgraduate Studies in Petroleum Geology, Faculty of Engineering, University of Zulia, Maracaibo 10482, Venezuela; escomar24@gmail.com
2 Department of Mining, Mechanical, Energetic and Civil Engineering, University of Huelva, 21819 Huelva, Spain; gonzalo.marquez@diq.uhu.es (G.M.); p.marinbarba@gmail.com (P.M.); romaci@uhu.es (E.R.)
3 PDVSA Western Division, Department of Exploration and Production, Maracaibo 4002, Venezuela; guerrerob@pdvsa.com
4 Department of Mining Technology, Topography and Structures, University of León, 24071 León, Spain; antonio.bernardo@unileon.es
5 Department of Mineralogy, Petrology and Applied Geology, University of Barcelona, 08028 Barcelona, Spain; albert.permanyer@ub.edu
* Correspondence: carlos.boente@dimme.uhu.es

Received: 16 September 2020; Accepted: 20 October 2020; Published: 27 October 2020

Abstract: The organic geochemical features of 30 sampled oils from the northern Bolivar Coastal Complex (Lake Maracaibo Basin, NW Venezuela) were examined by combining carbon isotope, classical biomarker, and extended diamondoid analyses to clarify source facies and to assess the thermal maturity and extent of biodegradation of the oils analyzed. In this work, oils are understood as a mixture of two episodes of petroleum generation from the La Luna Formation: a paleobiodegraded oil pulse during Paleogene times and a late pulse having a higher maturity in the post-Oligocene. For the oil samples analyzed, results revealed a mixing composed of different proportions of almost a terrestrially derived siliciclastic-sourced and a purely marine carbonate-sourced oil pulse. Moreover, two main groups of oils were identified by means of hierarchical cluster analysis. Finally, inter- and intrafield variations in the extent of biodegradation were also assessed using two classification schemes (Peters and Moldowan, and Manco scales).

Keywords: mixed oils; source facies; QEDA analysis; biodegradation scales; Bolivar Coastal Complex

1. Introduction

The Lake Maracaibo Basin (NW Venezuela) is among the world's most productive petroleum producing regions. It covers approximately 50,000 km^2, with the Upper Cretaceous La Luna Formation its principal source rock, although others have also been identified in the region [1,2]. Within the basin, oils are ubiquitous and mainly accumulated in Eocene and Miocene sandstones [3]. In the eastern edge of Lake Maracaibo, the basin is situated the area called Bolivar Coastal Complex (Figure 1) [4], consisting of a series of oilfields (Punta Benítez, Lagunillas, Bachaquero, etc.), two of which are the northernmost Tía Juana Lago and Cabimas, which cover about 210 and 136 km^2, respectively, and contain around 17.3 and 2.2 billion barrels of petroleum on-site [5,6]. Previous geochemical works [1,3,7] indicate that the La Luna Formation (upper Cenomanian–upper Campanian) comprises limestones interbedded with marlstones and large amounts of predominantly marine amorphous organic matter (Total Organic

Carbon (TOC) ranging from 2.5 to 10.8% wt.). This unit was deposited under reducing conditions in a middle to outer neritic environment on the northwest part of South America [8,9]. Two primary organic-rich La Luna Formation sedimentary facies can be distinguished on the basis of the percentage of shale present: more than 50% shale in the southern part of the basin, falling below 50% shale in other parts of the basin [10]. In terms of organic facies, the La Luna Formation is more carbonatic towards the north, grading southeastward into more siliciclastic facies throughout the southern Lake Maracaibo Basin and northern part of the Apure/Barinas Basin, along the alignment of the current Mérida Andes [7,11]. Differences between the La Luna "shale-rich" and "limestone-rich" facies are interpreted as a response to variations in continental runoff and also in concentration of molecular oxygen at the deepest part of the water column [12].

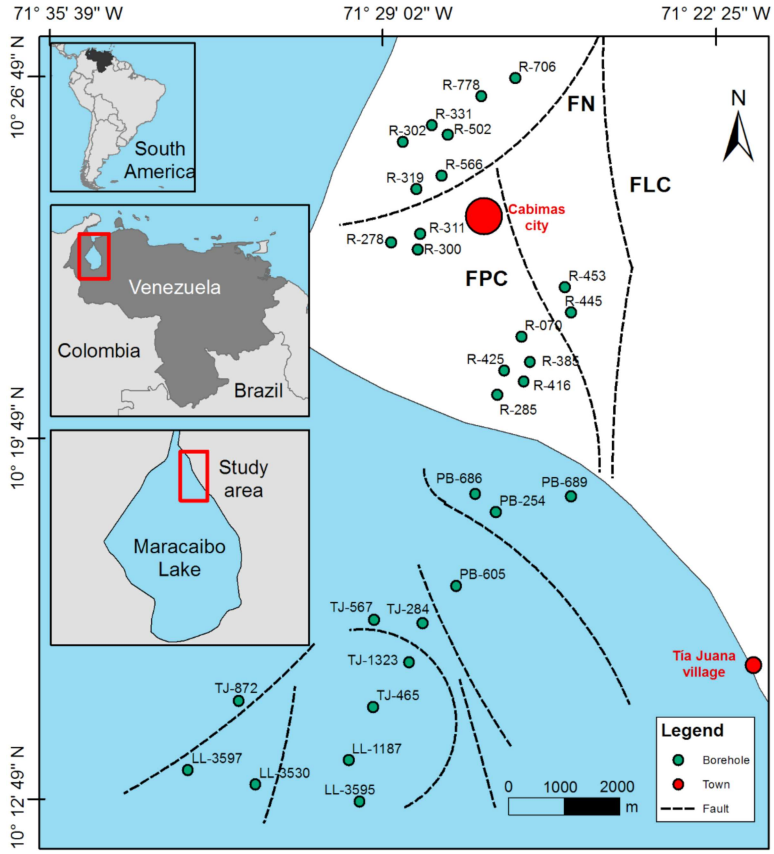

Figure 1. Northern Bolivar Coastal Complex map. It shows the location of the study oil wells.

Throughout the study area, altered oils occur in Miocene, Oligocene, and Upper Eocene reservoirs. These oils have been subjected to biodegradation, showing partial or complete absence of *n*-paraffins, high content in sulfur (>1.3%), low API (<25°), and aromatic/saturated proportions exceeding 0.5 [1]. The major part of mixed oils accumulated in the eastern side of Lake Maracaibo was generated from La Luna source kitchens at Neogene times, which dissolved the earlier paleobiodegraded Eocene oil charge during migration [13–15]. So far, oil–oil correlations have not unambiguously determined whether these mixed oils were generated from both aforementioned primary La Luna source facies.

The extent of petroleum biodegradation in the study area varies significantly; some oils show degradation of hopanes and steranes with occurrence of 10-demethylated hopanes and others do not [1]. Such variation in biodegradation levels and alteration pathways should be taken into account when implementing enhanced oil recovery techniques [16,17]. Microbial hydrocarbon degradation is influenced by aspects like the initial petroleum components, mixing of oil charges, microbial consortia, bottom water salinity, and nutrient supply [18–20]. In this study, as both the mixing of oils and biodegradation are commonly problematic in the Bolivar Coastal Complex, it may be useful to combine

at least two schemes for biodegradation assessment among the existing biomarker biodegradation scales, based on the depletion/absence of selected aromatic and saturated compound classes with different biorecalcitrance [21–24], in order to characterize with sufficient resolution the extent of such biodegradation in relation to mixed oil charges.

Thus, this project was carried out using thirty oil samples, which were collected from the Icotea, Lagunillas, and La Rosa reservoirs of the onshore Cabimas field, and from the Misoa B6 and B7 reservoirs of the offshore Tía Juana Lago area. The objectives of the present work are (i) to offer a better understanding about the origins and thermal maturity of oil samples, (ii) to determine whether sampled oils were generated from the primary La Luna "shale-rich" and/or "limestone-rich" source facies, (iii) to assess the level of biodegradation using PM [22] and Manco scales, and (iv) to evaluate possible inter- and intrafield changes in level of biodegradation.

2. Geological Features

The geology of the NW Venezuelan margin is constrained throughout interrelation of the Caribbean, North American, and South American plates [25]. Considering this framework, several geologists [26–29] have separated the sedimentary rocks in the E edge of Lake Maracaibo into various stratigraphic sections: (i) a passive margin sequence of Cretaceous age; (ii) a gradation to a compressive regime during the Early Paleocene and Late Cretaceous, when the South American plate was overridden by collision/obduction of the Pacific volcanic arc and the Lara nappes were emplaced; (iii) a Late Paleocene to mid-Eocene oblique convergence between a Caribbean island arc moving towards the west and the passive margin of South America, producing a foreland basin succession; and (iv) a sequence of Late Eocene to Pleistocene age in relation to the collision between the Panama arc and the South American plate.

Structurally, the geology of the Cabimas oilfield is characterized by homoclinal strata gently dipping to the southwest (3–8°) with a north orientation. The two principal structures are the NW–SE trending Prevalente (FPC) and Límite (FLC) fault systems (Figure 1), which were reactivated and inverted during the Andean compression. The Cabimas oilfield is limited to the east by the FLC structure, while a NE–SW trending normal fault transverse to the aforementioned structures (termed as the North Fault or FN) dips to the south and separates the Guzmán Flank from the rest [6]. To the north, the Guzmán Flank corresponds to a north–south trending faulted anticline [30]. Furthermore, a set of secondary structures are NE–SW trending en echelon normal faults perpendicular to the FPC and FLC faults; they all originated by compressive events in the Tertiary uplift history of the Venezuelan Andes [31]. Regarding the Tía Juana Lago area, the local structure is an asymmetrical anticline gently dipping to the southwest, with the crest to the northeast and the eastern flank of the fold to the southwest. Faulting within this area consists of a set of normal secondary faults not affecting the Eocene strata (see Figure 1; [5]).

The stratigraphic column of both study areas comprises Cretaceous and Tertiary sedimentary rocks (Figure 2) and presents the following lithologies, ordered from bottom to top: the arkosic sands of the Río Negro Formation; Apón (shales/gray limestones) unit; Lisure (sandstones interbedded with shales and limestones rich in glauconite); the Cogollo Group consisting of the Maraca (limestones rich in fossil debris); La Luna (marlstones and black limestones); Colón (dark shales); Mito Juan (siltstones); Guasare (sandstones and limestones); Misoa (sandstones, lutites, limonites, and limestones); Icotea (limonites, sandstones, and claystones); La Rosa (sandstones interbedded with fossiliferous shales); Lagunillas (shales, coals, sandstones, and claystones); La Puerta (sandstones, claystones, and shales); Onia (siltstones, sandstones, claystones), and; lastly, El Milagro (conglomerates and sandstones) [5,6].

One of the producing intervals is the Misoa Formation, split into some subunits called sands "B", and "C", from top to bottom [32]. Subsequently, "C" sands are separated into seven minor subunits, indicating a transition from a distal deltaic (C4–C7) depositional environment to a prodelta (C1–C3) [33]. In turn, "B" sands are divided in nine minor subunits (B1–B9), indicating an evolution from a continental deltaic (B6–B9) to a restricted littoral–subtidal (B1–B5) environment [34].

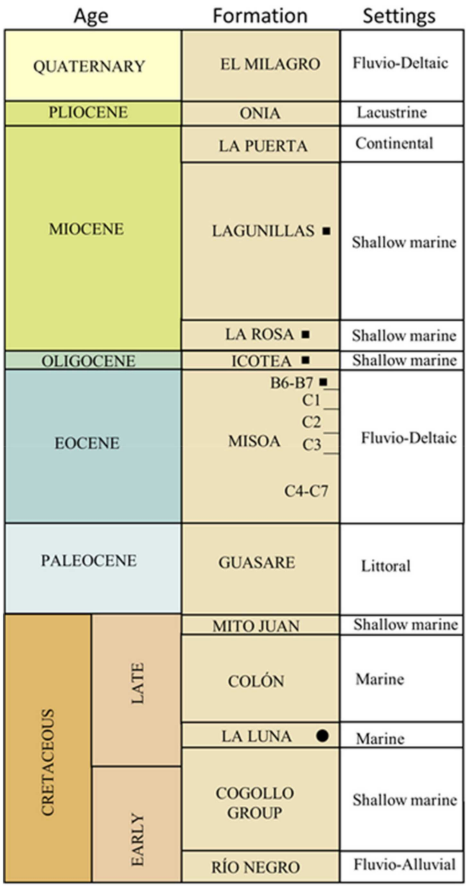

Figure 2. Stratigraphic units in the northern Bolivar Coastal Complex. Note: black circles and black squares indicate source rocks and reservoir intervals, respectively.

3. Materials and Methods

Thirty samples of oil from the Eocene, Oligocene, and Miocene reservoirs in the Cabimas field and Tía Juana Lago sector were studied (Table 1 and Figure 1). American Petroleum Institute (API) gravities of oil samples were measured according to the D287-92 standard [35]. Sulfur was measured in accordance with ASTM D4294-10 standard procedure [36]. A part of each sample was fractionated into aromatics (ARO), saturates (SAT), and asphaltenes plus resins (POL). First, asphaltenes were isolated using *n*-heptane in a ratio of 1:40 *v/v* in accordance with Speight [37]. The asphaltenes were separated in a Soxhlet extractor using 0.45-µm filters and *n*-heptane as solvent, in a process that was repeated until obtaining colorless filtrates. Secondly, maltenes were separated into aromatic, saturated, and resin fractions through liquid chromatography using columns filled with alumina and silica gel [38]. In order to elute these fractions, respectively, *n*-hexane, dichloromethane/hexane (7:3 *v/v*), and dichloromethane/methanol (1:1, *v/v*) were used as solvents.

Carbon isotopic values of aromatic and saturated fractions were determined through a Thermo Finnigan 1112 elemental analyzer combined with a Finnigan Mat Delta C mass spectrometer. USGS 24 graphite, IAEA-CH7 polyethylene, NBS-22 oil, and IAEA-CH6 saccharose were the reference materials. The 13C/12C ratio is described by "δ" notation while $\delta^{13}C$ refers to PDB standard (Pee Dee belemnite).

Aromatic and saturated compounds were investigated through gas chromatography–mass spectrometry (GC–MS). The GC–MS studies were achieved using a 5975C Inert XL MSD carrying Triple-Axis Detector (Agilent Technologies) coupled with an Agilent's 7890A GC. These instruments run with helium as carrier gas. Gas chromatography was done with an Agilent capillary column DB-5 ms (60 m × 0.25 mm i.d. × 0.10 µm film thickness). Initially, the oven temperature was 50 °C for 2 min, and ramped at 2.5 °C until reaching 300 °C, holding for 70 min. Ionization operated in electronic impact mode (EI) with 70 eV of electron energy. MS autotune/calibration was performed once per

day. The chromatograms were collected in single-ion monitoring and full-scan modes (mass range acquisition was carried out from *m/z* 45 to 500). SPSS 19.0 software package was used for multivariate statistical analysis.

Table 1. Reservoir names, depths, bulk composition, API gravities, sulfur contents (wt.%), and $\delta^{13}C$ data (‰) of the aromatic and saturated hydrocarbons (wt.%) of the oils analyzed.

Well	Depth	Interval	St	SAT	ARO	POL	°API	$\delta^{13}C_{ARO}$	$\delta^{13}C_{SAT}$
R-070	505	La Rosa	1.68	40	30	30	25	−26.15	−27.14
R-278	652	Icotea	1.97	36	29	35	20	−26.49	−27.33
R-285	588	La Rosa-Icotea	1.79	40	30	30	23	-	-
R-300	661	La Rosa-Icotea	1.94	36	30	34	20	−26.35	−27.50
R-302	401	Lagunillas-La Rosa	2.20	34	28	38	16	-	-
R-311	434	Lagunillas-La Rosa	2.14	34	26	38	18	-	-
R-319	640	Lagunillas-La Rosa	2.15	37	29	34	20	-	-
R-331	478	Lagunillas-La Rosa	2.05	37	28	35	21	-	-
R-385	438	La Rosa	1.85	41	30	29	24	−26.42	−27.58
R-416	389	La Rosa	1.63	41	30	29	26	-	-
R-425	395	La Rosa	1.75	40	30	30	23	−26.33	−27.55
R-445	354	La Rosa	1.90	38	29	33	22	-	-
R-453	372	La Rosa	1.88	40	32	28	22	-	-
R-502	353	Lagunillas-La Rosa	2.03	36	29	35	19	-	-
R-566	535	La Rosa-Icotea	1.91	38	29	33	21	-	-
R-706	312	Lagunillas	2.22	34	30	36	17	-	-
R-778	324	Lagunillas	2.29	34	29	37	17	−26.20	−27.16
TJ-1323	1407	Misoa B6	0.97	48	27	25	35	−26.38	−27.98
TJ-567	1547	Misoa B6	-	37	29	34	23	-	-
TJ-872	1392	Misoa B6	0.93	48	27	25	34	−26.46	−27.81
TJ-465	1206	Misoa B6	-	40	29	31	26	−26.37	−27.72
LL-3597	1357	Misoa B6	-	41	28	31	26	-	-
PB-686	1939	Misoa B6	1.45	39	29	32	24	-	-
PB-689	1893	Misoa B6	-	34	30	36	21	-	-
PB-254	1797	Misoa B6	1.54	35	29	36	21	−26.24	−27.51
PB-605	1564	Misoa B6	-	36	28	36	22	-	-
TJ-284	1713	Misoa B6	-	34	28	38	21	−26.41	−27.67
LL-3530	1352	Misoa B7	1.28	46	28	26	28	-	-
LL-1187	1275	Misoa B7	-	45	28	27	29	−26.38	−27.78
LL-3595	1274	Misoa B7	-	45	29	26	28	−26.19	−27.52

Note: depth expressed in meters.

Finally, quantitative analysis of extended diamondoid (QEDA) was carried out on saturated hydrocarbon fraction from two representative sampled oils through gas chromatography–triple quadrupole mass spectrometry [39,40]. In detail, QEDA fingerprints were examined in the corresponding pyrolysates after hydrous pyrolysis of asphaltenic fractions of these sampled oils was performed on the basis of the methodology established by Summons [41]. Quantification of triamantane molecule and extended polimantanes was done using four deuterated internal standards, particularly cyclohexamantane-d8 and triamantane-d4, in addition to pentamantane-d6 and tetramantane-d6 for the five-cage (P1, P2, P3, and P4) and four-cage (T1, T2, and T3) non-enantiomorphic isomers. Structures of penta-, tetra-, and hexamantane (H1) molecules studied are shown in [42].

4. Results and Discussion

4.1. Bulk Data and SARA Composition

Bulk geochemical data including the Saturate, Aromatic, Resin Asphaltene (SARA) composition, total sulfur, and API value of each sampled oil are displayed in Table 1. All the oils analyzed excluding

TJ-872, TJ-1323, and those from the Misoa B7 interval showed API values from 16 to 26° and relatively similar SARA contents: SAT in the 34–41% range, ARO ranging from 26% to 30%, and POL ranging between 30% and 38%. As second group of oils, namely, the samples from the Misoa B7 interval displayed API values, ARO, SAT and POL weight percents in the 28–29°, 28–29%, 45–46%, and 26–27% ranges, respectively. A last group comprises TJ-872 and TJ-1323 oils from the Misoa B6 interval, and both showed identical ARO proportions (27%), the highest measured API gravities (>34°) and SAT proportions (48%), as well as the lowest POL percentages (25%). These data correspond to normal oils in accordance with [43]. As for total sulfur contents, most oil samples depicted values exceeding 1% wt., except for TJ-872 and TJ-1323 (Table 1). Variances in these datasets may be explicated by biodegradation [44], as discussed below.

4.2. Carbon Isotope Signature

The carbon isotope values of the aromatic and saturated fractions of sampled oils are similar among them (see Table 1), with standard deviations approaching the analytical error (0.5‰), thereby suggesting that all sampled oils were derived from the same source rocks [45]. When considering the Sofer diagram ([46], Figure 3), the $\delta^{13}C$ values for the oils analyzed plot in the marine organic matter region, which is consistent with these samples being sourced from the marine organic materials of the La Luna rock unit, in line with previous studies indicating that the La Luna rock unit is the primary source rock of the region [14,15]. Nevertheless, these data must be interpreted cautiously as several secondary processes can alter the carbon isotopic signature [47].

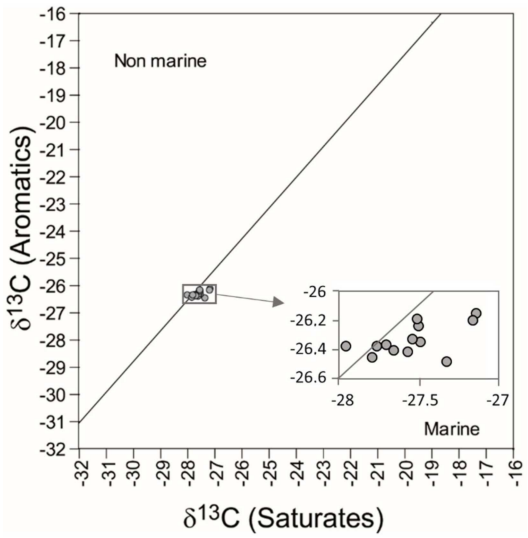

Figure 3. Sofer isotope diagram for the aromatic and saturated hydrocarbons of thirteen representative oil samples.

4.3. In-Reservoir Biodegradation

Total ion current (TIC) chromatograms of the saturated hydrocarbons of two representative sampled oils are exhibited in Figure 4, revealing the existence of an "unresolved complex mixture" related with naphthenic compounds produced through biodegradation processes [48]. API values below 35° may also be indicative of microbial degradation [16], and/or may be suggestive of a mixture of two or more petroleum charges. The latter option agrees with two main episodes of petroleum expulsion from the La Luna source rocks on the eastern margin of Lake Maracaibo, as described in previous studies [14,15]; an early generation pulse of oil occurred in the Middle Eocene—this oil would have been paleobiodegraded during Late Eocene age and mixed with a recharge of unaltered oil during the Neogene [1]. The proportion of these two oil charges may explain the wide variability of API gravity in the samples.

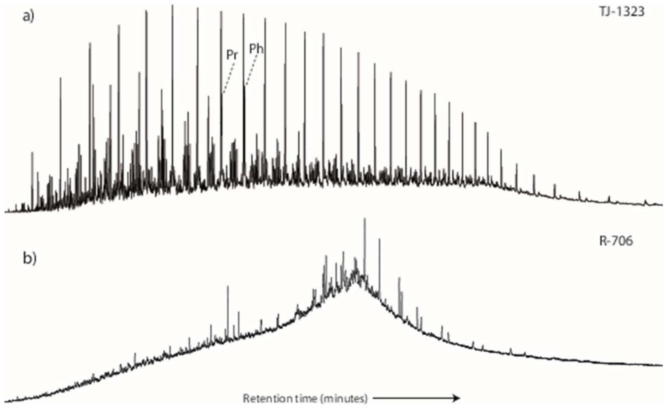

Figure 4. Total ion chromatogram of the saturated fraction of TJ-1323 (**a**) and R-706 (**b**) oils.

The 10-demethylhopanes are ubiquitous in all the oil samples (*m/z* 191 and 177 fragmentograms of characteristic oil samples are exhibited in Figure 5; peak identifications are listed in Appendix A). The presence of these biological markers indicates heavy biodegradation and is described in literature as caused by the modification of the C_{10} methyl group in the hopanes [49]. Nevertheless, most samples contain 10-demethylhopanes along with *n*-paraffins/isoprenoids (see Table 2). The fact that compounds of such different recalcitrance coexist in oils is here explained by assuming that 10-demethylhopanes formed by paleobiodegradation of the hydrocarbon liquids generated during the Eocene, which were mixed with fresher oil charge(s) formed in post-Paleogene times [45]. Since all the less recalcitrant hydrocarbons would be attributable to the late oil charge, ratios of pristane to C_{17} *n*-alkane exceeding 0.5 (see Table 3) in most oil samples suggest that the late oil charge would have suffered only little to moderate microbial degradation [50].

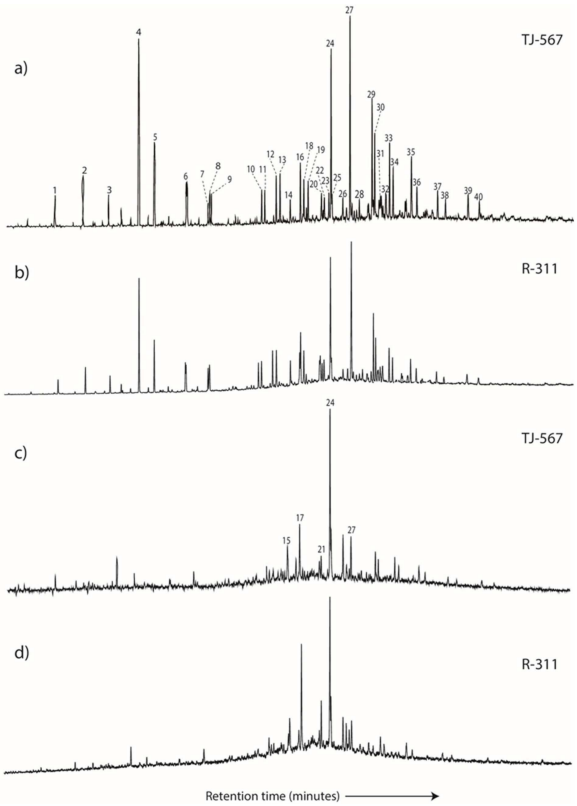

Figure 5. Examples of *m/z* 191 (**a**,**b**) and *m/z* 177 (**c**,**d**) ion chromatograms of the saturated fraction of representative TJ-567 and R-311 oils.

Table 2. PM and Manco biodegradation levels of the oils analyzed.

Sample	C_1–C_{14} *n*-alk	C_{15+} *n*-alk	IsoP	Alkyl-tol	N + MN	DMN	UMN1	PM
R-070	Depleted	Affected	Near-intact	Near-intact	Near-intact	Intact	9766413	2/6
R-278	Absent	Absent	Depleted	Depleted	Depleted	Near-intact	9771099	4/6
R-285	Absent	Depleted	Near-intact	Near-intact	Depleted	Near-intact	9770794	3/6
R-300	Absent	Absent	Depleted	Depleted	Affected	Near-intact	9770474	4/6
R-302	Absent	Absent	Absent	Absent	Absent	Affected	9774999	5/6
R-311	Absent	Absent	Absent	Absent	Absent	Affected	9774999	5/6
R-319	Absent	Absent	Depleted	Depleted	Depleted	Near-intact	9771099	4/6
R-331	Absent	Absent	Depleted	Depleted	Depleted	Near-intact	9771099	4/6
R-385	Absent	Absent	Near-intact	Near-intact	Depleted	Near-intact	9770799	3/6
R-416	Depleted	Affected	Near-intact	Near-intact	Near-intact	Intact	9766413	2/6
R-425	Absent	Depleted	Near-intact	Near-intact	Depleted	Near-intact	9770794	3/6
R-445	Absent	Absent	Near-intact	Near-intact	Depleted	Near-intact	9770799	3/6
R-453	Absent	Depleted	Near-intact	Near-intact	Depleted	Near-intact	9770794	3/6
R-502	Absent	Absent	Depleted	Depleted	Depleted	Near-intact	9771099	4/6
R-566	Absent	Absent	Depleted	Depleted	Affected	Near-intact	9770474	4/6
R-706	Absent	Absent	Absent	Absent	Absent	Affected	9774999	5/6
R-778	Absent	Absent	Absent	Absent	Absent	Affected	9774999	5/6
TJ-1323	Near-intact	Intact	Intact	Intact	Intact	Intact	9774287	1/6
TJ-567	Affected	Near-intact	Intact	Intact	Intact	Intact	9774349	2/6
TJ-872	Near-intact	Intact	Intact	Intact	Intact	Intact	9774288	1/6
TJ-465	Affected	Near-intact	Intact	Intact	Intact	Intact	9778099	2/6
LL-3597	Affected	Near-Intact	Intact	Intact	Intact	Intact	9778124	2/6
PB-686	Near-intact	Intact	Intact	Intact	Intact	Intact	9778124	1/6
PB-689	Near-intact	Intact	Intact	Intact	Intact	Intact	9778099	1/6
PB-254	Near-intact	Intact	Intact	Intact	Intact	Intact	9778099	1/6
PB-605	Affected	Near-Intact	Intact	Intact	Intact	Intact	9777413	2/6
TJ-284	Near-intact	Intact	Intact	Intact	Intact	Intact	9774287	1/6
LL-3530	Affected	Near-Intact	Intact	Intact	Intact	Intact	9774913	2/6
LL-1187	Affected	Near-Intact	Intact	Intact	Intact	Intact	9778069	2/6
LL-3595	Affected	Near-Intact	Intact	Intact	Intact	Intact	9778069	2/6

Notes: Given any compound class, intact, near-intact, affected, depleted, and absent correspond to 0–4 Manco scores, respectively. C3- and C4-naphthalenes, methyldibenzothiophenes, and phenanthrene series remain practically intact in all the samples, while regular steranes are slightly altered.

A more precise biodegradation study can be done using PM [22] and Manco [24] scales. Based on the PM scale, the earlier charge of oil would be ranked at 6, for all oil samples, due to the presence of 25-norhopanes and the slight alteration of regular steranes (see Figure 6), specifically the ααα20R and αββ20R C29 homologues [51], leading to ratios of pregnane to ααα20R stigmastane higher than 0.5 [52]. Nevertheless, differences are seen between sampled oils when assessing the biodegradation of the later oil charge. As mentioned, for some samples, it is evident the partial depletion of *n*-paraffins and no or minor alteration of isoprenoidal alkanes in numerous oil samples (Table 2), suggesting a PM degradation level of 1–2. By contrast, R-302, R-311, R-706, and R-778 oils completely lack isoprenoids and *n*-paraffins such as phytane and pristane (PM level of 5). A latter set of samples have a significant or near-total lack of *n*-paraffins/isoprenoids, which is consistent with a PM level of 3–4. Variances in the alteration levels of normal and isoprenoidal alkanes in the oil samples might be explicated by distinct reasons such as the existence of different reservoir temperatures and microbial associations, the inflow of pristine oil within reservoir subcompartments, or the rates of microbial degradation [18,20].

Table 3. Molecular parameters obtained from the aromatic and saturated hydrocarbons of the oils analyzed, which indicate source types and depositional environments.

Sample	%27ST	%28ST	%29ST	Ts/Tm	Ph/nC_{18}	Pr/nC_{17}	Pr/Ph	29/30H	31R/30H	26/25T	24/23T	DBT/P	Dia/ST
R-070	37	32	31	0.51	0.78	0.68	0.61	0.93	0.42	0.86	0.47	0.90	0.20
R-278	36	33	31	0.49	-	-	-	0.84	0.39	0.90	0.43	0.92	0.22
R-285	38	32	30	0.52	-	-	0.62	0.86	0.41	0.89	0.45	0.94	0.21
R-300	37	33	30	0.48	-	-	-	0.82	0.42	0.91	0.44	0.91	0.22
R-302	37	32	31	0.50	-	-	-	0.90	0.38	0.85	0.43	0.89	0.20
R-311	35	33	32	0.52	-	-	-	0.83	0.40	0.88	0.48	0.95	0.23
R-319	35	33	32	0.49	-	-	-	0.91	0.41	0.87	0.49	0.90	0.21
R-331	39	32	29	0.53	-	-	-	0.85	0.38	0.85	0.49	0.93	0.20
R-385	36	33	31	0.47	-	-	0.63	0.87	0.40	0.90	0.47	0.95	0.23
R-416	37	32	31	0.50	0.75	0.66	0.67	0.93	0.39	0.86	0.44	0.94	0.21
R-425	35	33	32	0.52	-	-	0.64	0.79	0.37	0.89	0.45	0.96	0.20
R-445	36	33	31	0.48	-	-	0.66	0.90	0.41	0.92	0.46	0.88	0.21
R-453	37	32	31	0.53	-	-	0.65	0.88	0.43	0.89	0.48	0.92	0.22
R-502	35	33	32	0.49	-	-	-	0.92	0.36	0.86	0.44	0.94	0.22
R-566	38	32	30	0.51	-	-	-	0.80	0.39	0.91	0.43	0.91	0.22
R-706	37	33	30	0.48	-	-	-	0.91	0.42	0.83	0.41	0.98	0.23
R-778	36	33	31	0.51	-	-	-	0.85	0.42	0.84	0.42	0.93	0.21
TJ-1323	36	33	31	0.66	0.48	0.39	0.84	0.79	0.42	0.91	0.49	0.78	0.25
TJ-567	37	34	29	0.46	0.68	0.53	0.71	0.87	0.43	0.89	0.41	0.88	0.21
TJ-872	37	32	31	0.64	0.49	0.40	0.81	0.79	0.42	0.90	0.48	0.77	0.25
TJ-465	39	32	29	0.48	0.72	0.62	0.75	0.91	0.38	0.85	0.43	0.86	0.22
LL-3597	38	32	30	0.50	0.67	0.53	0.74	0.94	0.43	0.86	0.44	0.90	0.21
PB-686	37	33	30	0.46	0.59	0.41	0.68	0.92	0.41	0.92	0.43	0.91	0.21
PB-689	35	33	32	0.52	0.60	0.46	0.70	0.93	0.38	0.85	0.45	0.97	0.20
PB-254	38	33	29	0.48	0.59	0.48	0.71	0.83	0.39	0.86	0.46	0.92	0.20
PB-605	37	33	30	0.51	0.71	0.56	0.66	0.85	0.37	0.90	0.43	0.93	0.22
TJ-284	37	32	31	0.54	0.59	0.49	0.66	0.90	0.36	0.86	0.42	0.91	0.21
LL-3530	38	32	32	0.60	0.68	0.54	0.86	0.81	0.38	0.87	0.45	0.81	0.23
LL-1187	37	32	31	0.61	0.70	0.57	0.82	0.80	0.40	0.89	0.47	0.80	0.23

Notes: 29/30H = 30-norhopane/hopane; 24/23T = C_{24}-cheilanthane/C_{23}-cheilanthane; Dia/ST = diasterane ratio or C_{27}-diasteranes/C_{27}-normal steranes; %27ST = percentage of C_{27} regular steranes; Pr/Ph = pristane/phytane; Pr/nC_{17} = pristane/*n*-heptadecane; 31R/30H = homohopane 22R/hopane; DBT/P = dibenzothiophene/phenanthene; 26/25T = C_{26}-tricyclopolyprenanes/C_{25}-tricyclopolyprenane; ST/30H = ratio of C_{29}-normal steranes to C_{30}-hopane; and Ts/Tm = 18α(H)-22,29,30 trisnorneohopane/17α(H)-22,29,30 trisnorhopane.

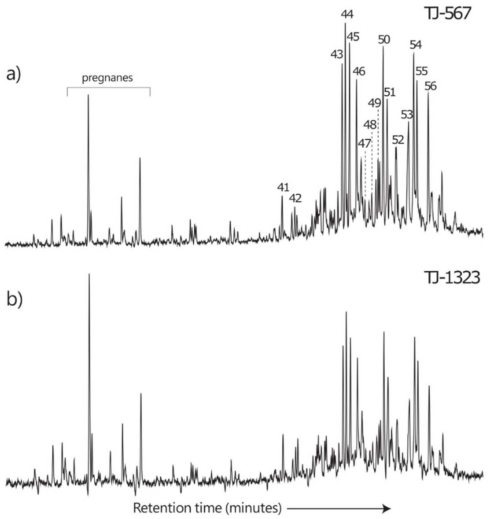

Figure 6. The *m/z* 217 ion chromatograms of the saturated hydrocarbons of representative TJ-567 (**a**) and TJ-1323 (**b**) oils showing sterane distributions.

As for the Manco scale, Figures 7 and 8 show examples of the distribution of seven out of the eight primary Manco compound classes reflecting increasing recalcitrance (see [24]) for representative oils analyzed. All the samples are characterized by displaying the preservation and similar distribution of various compound classes: multialkylated naphthalenes, phenanthrene series, and steranes. Thus, the naphthalene series is characterized by showing low abundances of the most recalcitrant 2,3-, 1,2,4-, and 1,2,5,6+1,2,3,5-isomers (Figure 7c; [53,54]) in numerous samples. Instead, differences among the oil samples can be observed in the distribution of *n*-paraffins/isoprenoids, alkyltoluenes, and $C_{0–1}$ naphthalenes. These latter compound classes remain intact or slightly altered in all the samples from the Misoa B6/B7 reservoir interval at 65–70 °C, while in the oils from the Icotea, La Rosa, and Lagunillas reservoirs at 30–40 °C, these compounds are partially to fully degraded (Table 2). The lack or loss of alkyltoluenes in the oils from the Cabimas area could suggest that these oils can only be produced by thermal recovery in the Cabimas area [24]. Noteworthy also is that all the samples show noncorrelative PM levels of biodegradation (see Table 2). In this regard, prior studies have reported seepage oils depicting uncorrelated levels of biodegradation (e.g., [55]). Anomalous degradation trends are observed in sampled oils and may be the result of adding unaltered oil to a previously biodegraded hydrocarbon liquid [56].

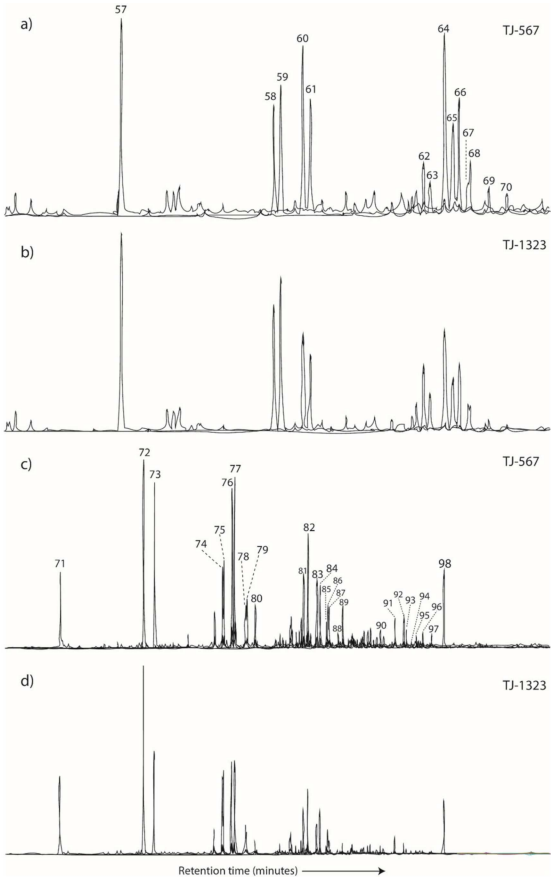

Figure 7. For TJ-567 and TJ-1323 oils, *m/z* 178 + 192 + 206 (**a**,**b**) and *m/z* 128 + 142 + 156 + 170 + 184 (**c**,**d**) ion chromatograms of the aromatic fraction. Phenanthrene and naphtalene series distributions are shown.

Table 2 also contains the Manco scores for the calculation of the ultimate Manco values (UMN1 and UMN2), which generally tend to be useful for discriminating between oils of PM levels ranging from 0 to 7 [24]. For this, eleven compound classes were established, which in increasing order of resistance to biodegradation are short-chain *n*-alkanes, C_{15+} *n*-alkanes, isoprenoid alkanes, alkyltoluenes, $C_{0–1}$-naphthalenes, C2-naphthalenes, C3-naphthalenes, methyldibenzothiophenes

(MDBT), C_4-naphthalenes, phenanthrene series, and steranes. UMN2 was used to define the Manco level of degradation. Firstly, the ion chromatograms of these compound classes were visually examined to assign a score to each compound category, based on how much degradation they had suffered (between 0–4; representing imperceptibly, slightly, moderately, heavily, and fully degraded components, respectively). Then, each compound class score was achieved when multiplying the respective Manco score by 5 raised to a number ranging between 0 and 10 in increasing resistance-to-biodegradation order. The summation of the compound class scores is the UMN1 value [24]. The UMN2 number (between 0–1000) is assigned a value of 0 if UMN1 equals 0, or otherwise is calculated as one plus 999 (the scale maximum minus one) multiplied by the quotient between the log (base 5) of UMN1 and 11 (the number of compound classes). The oil samples have UMN2 values of about 909, with very little variation. This is interpreted as reflecting information only of the paleobiodegraded phase of the mixed sampled oils, as both the UMN1 and UMN2 numbers are mainly controlled by the score of the most recalcitrant compound class (regular steranes in the oils analyzed) that are affected by microbial degradation.

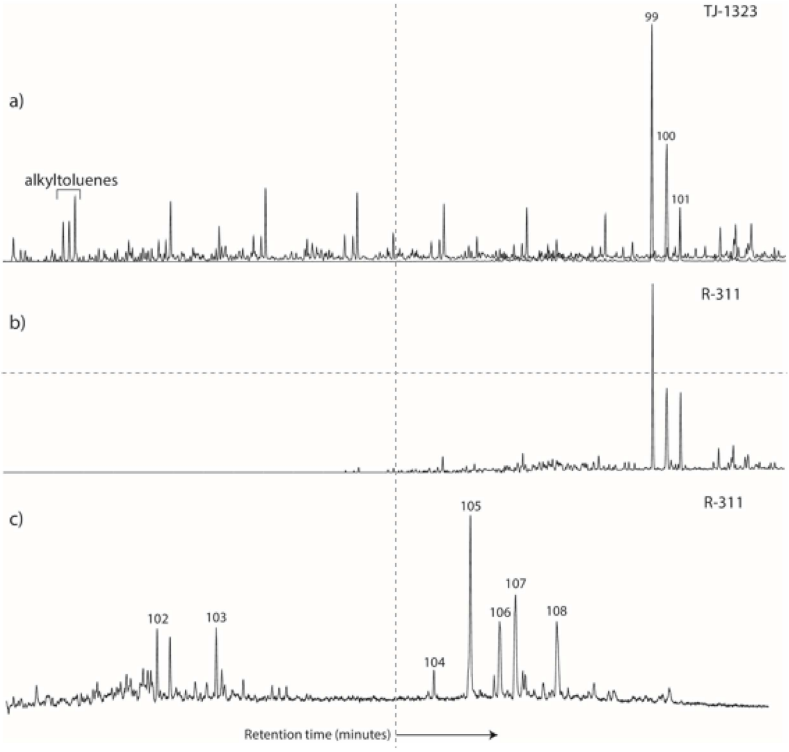

Figure 8. The *m/z* 105 + 198 ion chromatograms of the aromatic fraction for TJ-1323 (**a**) and R-311 (**b**) oils showing methyldibenzothiophene and alkyltoluene distributions; (**c**) representative *m/z* 231 ion fragmentogram of the aromatic fraction of the R-311 oil showing the triaromatic steroidal hydrocarbon distribution.

4.4. Thermal Maturity

Molecular maturation indicators for aromatic and saturated hydrocarbons of the oil samples are shown in Table 4. Nevertheless, given the aforementioned mixing of oil charges, these indices (excluding the methylphenanthrene ratio) are applied cautiously [45].

Table 4. Maturity-related molecular ratios of aromatic and saturated fractions in oils analyzed.

Sample	%20*S*	%ββ	Rc_1	TA	Rc_2	MPR	Rc_{33}	MPI-1	Rc_4
R-070	55	58	0.78	0.29	0.75	1.11	0.98	0.75	0.85
R-278	57	56	0.76	0.27	0.74	1.15	1.00	0.76	0.85
R-285	56	59	0.79	0.28	0.74	1.20	1.02	0.76	0.85
R-300	57	59	0.79	0.26	0.73	1.14	0.99	0.79	0.87
R-302	55	57	0.77	0.26	0.73	1.17	1.01	0.79	0.87
R-311	56	57	0.77	0.27	0.74	1.24	1.03	0.78	0.87
R-319	58	56	0.76	0.28	0.74	1.22	1.02	0.75	0.85
R-331	56	58	0.78	0.29	0.75	1.14	0.99	0.82	0.89
R-385	58	59	0.79	0.27	0.74	1.13	0.99	0.80	0.88
R-416	56	57	0.76	0.28	0.74	1.15	1.00	0.76	0.85
R-425	58	57	0.76	0.27	0.74	1.18	1.01	0.77	0.86
R-445	57	58	0.78	0.29	0.75	1.16	1.00	0.75	0.85
R-453	56	56	0.76	0.26	0.73	1.21	1.02	0.81	0.88
R-502	57	57	0.77	0.25	0.72	1.19	1.01	0.77	0.86
R-566	56	58	0.78	0.28	0.74	1.12	0.99	0.78	0.87
R-706	55	57	0.77	0.29	0.75	1.16	1.01	0.80	0.88
R-778	56	59	0.79	0.27	0.74	1.15	1.00	0.75	0.85
TJ-1323	48	52	0.70	-	-	1.17	1.01	1.07	1.05
TJ-567	49	51	0.70	0.27	0.74	1.16	1.01	0.80	0.88
TJ-872	48	52	0.70	-	-	1.23	1.03	1.08	1.05
TJ-465	48	52	0.70	0.29	0.75	1.12	0.99	0.83	0.90
LL-3597	49	53	0.71	0.28	0.74	1.27	1.04	0.78	0.87
PB-686	48	52	0.70	0.28	0.74	1.21	1.02	0.79	0.87
PB-689	48	52	0.70	0.25	0.72	1.18	1.01	0.81	0.89
PB-254	48	51	0.69	0.28	0.74	1.15	1.00	0.76	0.85
PB-605	49	53	0.71	0.26	0.73	1.20	1.02	0.79	0.87
TJ-284	48	52	0.70	0.26	0.73	1.17	1.01	0.77	0.86
LL-3530	52	54	0.76	0.28	0.74	1.25	1.04	0.86	0.91
LL-1187	52	55	0.76	0.25	0.72	1.16	1.01	0.87	0.92
LL-3595	51	54	0.75	0.27	0.74	1.10	0.98	0.85	0.91

Notes: %ββ = ratio(%) of C_{29} isosteranes (20S + 20R) to sitostanes (20S + 20R); $\%Rc_1 = 0.3333 + 0.00487 \cdot \%20S$; %20S = 5α,14α,17α(H)-sitostane 20S and 20R ratio(%); TA = C_{20+21} counterparts to C_{20+21} plus $C_{26+27+28}$ triaromatic steroidal ratio; $\%Rc_2$ calculated from the TA ratio in accordance with Mackenzie [57]; MPI-1 = 1.5·(2-MP + 3-MP)/(P + 1-MP + 9-MP); $Rc_4 = 0.4 + 0.6 \cdot$MPI-1 when $\%Rc_4$ ranges from 0.65 to 1.35% [58]; MPR = 2-MP/1-MP; and vitrinite reflectance based on the MPR ratio (0.94 + 0.99·log·MPR) [59].

Sterane isomerization parameters (%ββ and %20*S*) have been interpreted to rise, respectively, from 0–0.5 to 0.7 and 0 to 0.55 with thermal maturity increasing [57]. The oil samples showed %ββ and %20*S* values of 51–59% and 48–58% (Table 4), which could be coherent with a maturity level equivalent to the beginning of the peak oil generation [50]. The characteristic triaromatic steroid hydrocarbon peaks (see Figure 8c) were observed and close values of the triaromatic steroidal ratio for the oils analyzed (0.25–0.39; Table 4) were determined in all the oil samples, which would suggest maturation levels on the onset of oil generation [57]. Two methylphenanthrene-based ratios were calculated as well.

Regarding the methylphenanthrene ratio (MPR or ratio of 2- to 1-isomer), considered as a practical indicator of maturity level for marine organic material at vitrinite reflectances beyond 0.9% [59,60], the sampled oils showed very similar MPR values ranging from 1.1 to 1.27 (Table 4). This would denote a maturation level equivalent to about 1% after the peak oil generation. The fact that maturation levels obtained from the MPR ratio are similar, is interpreted here as reflecting the high susceptibility to biodegradation of 1- and 2-methylphenanthrene in comparison with the 3- and 9-isomers [61], thus the latter compounds would have been removed from the early biodegraded oil charge (Paleogene) before the presence of the 25-norhopanes [53]. Therefore, the MPR ratio (with equivalent vitrinite reflectance values of ~1%) assesses the maturity level of the late generation oil pulse (post-Oligocene). Instead, the MPI-1 index [58,62] shows differences between the oils analyzed; most samples, except for TJ-872 and TJ-1323, have MPI-1 values in the 0.75–0.87 range and, consequently, calculated vitrinite reflectances ranging between 0.85 and 0.92%. MPI-1 values denote maturation levels lower than that of the Neogene-Quaternary oil charge. This feature agrees with the predominance of the 9-MP over their most susceptible methylphenanthrene homologues in the paleobiodegraded liquid [54]. As for the TJ-872 and TJ-1323 oils, which have the highest MPI-1 values (1.07–1.08) with maturation levels equivalent to 1.05%, it is assumed that these two samples may represent a dominant contribution of the Late Neogene oil charge. The dominance of 2-methylnaphthalene over its isomer in TJ-872 and TJ-1323 samples is typical of mature oils (Figure 7c,d; [63]), although the 2-methylated homologue is more susceptible to biodegradation [53]. Another feature of the considerable thermal maturity is the high abundance of pregnanes relative to C27–C29 regular steranes [45].

4.5. Precursor Organic Material and Depositional Conditions

Several molecular parameters have been established to determine the type of organic material and some features of the paleoenvironment. The *n*-paraffin patterns for various oil samples were nearly identical among them, unimodal with maximum peaks from *n*-C_{16} to *n*-C_{18} (see Figure 4a), and characteristic of marine algal precursor organic matter [45]. Pristane/phytane (Pr/Ph) values range from 0.61 to 0.84 (Table 3), suggesting a precursor organic material that was deposited in anoxic conditions [43]. The Pr/Ph ratio might be biased by thermal maturation and other processes (e.g., [64]), but it may be used here to denote the depositional setting. For all the samples, Ph/*n*-C_{18} and Pr/*n*-C_{17} values (Table 3) agree with marine type-II organic matter (Hunt, 1996). Relatively high Ph/*n*-C_{18} and Pr/*n*-C_{17} (≥0.5) values may also indicate little biodegradation [45]. DBT/P values are lower than one in all the oil samples. When combined with total sulfur contents (St; [65]), in all the samples (except TJ-872 and TJ-1323 oils) marine carbonate/mixed marine settings would be inferred. Instead, the integration of the Pr/Ph and DBT/P ratios is not compatible with a marine carbonate sedimentary environment [65]. This apparent contradiction might be explained by water-washing of notably polar aromatic DBT [11]. In any case, it is assumed that all of the parameters obtained from C15+ *n*-alkanes, Pr, Ph, P, and DBT would only give information on the late oil charge, as these compounds would have been partially or fully removed from the earlier oil during paleobiodegradation [23,53].

Sampled oils presented similar sterane and triterpane distributions (Figures 5 and 6). Any *m/z* 191 ion chromatogram of the saturated hydrocarbons shows abundant cheilanthanes and a high quantity of C_{23} cheilanthane when compared to the C_{24} and other counterparts (Table 3), suggesting a precursor organic matter deposited in a marine setting [45]. High amounts of tricyclopolyprenanes could be explained by a high maturation of the late charge [66] and by the extent of alteration suffered by the paleobiodegraded hydrocarbon liquid [23]. Table 3 shows C_{26}/C_{25} cheillantane values below unity, C_{29}/C_{30} hopane and $C_{31}R/C_{30}$ hopane ratios >0.8 and >0.3, as well as values of 17a(H)-22,29,30 trisnorhopane/18a(H)-22,29,30 trisnorneohopane (Ts/Tm) < 1, which might indicate that these oils were generated from marine carbonate facies deposited under low-oxygen conditions [67–69]. Moreover, a typical *m/z* 217 ion chromatogram of the saturated hydrocarbons shows the predominance of C_{27} regular steranes with respect to the C_{29} and C_{28} homologues, as generally occurs in oil formed from

marine sources [68]. A predominantly carbonate source facies for the mixed oils under study is also revealed by low values (<0.26; see Table 3) of the quotient between diasteranes and regular steranes [70].

Regarding the methylated dibenzothiophenes, none of the oil samples presented the typical carbonate lithology distribution pattern (i.e., the coeluting 2- and 3-methyl isomers being the lowest [65]. Most samples exhibited a distribution pattern characterized by 4 > 2 + 3 > 1 (see Figure 8b). Instead, TJ-872 and TJ-1323 oils showed the common pattern for the MDBT homologues that corresponds to the siliciclastic lithology (4 > 2 + 3 > 1; see Figure 8a). These two oils also showed Ts/Tm values appreciably higher than most other samples (Table 3), which may also be suggestive of a more clayey source facies [69]. It is possible that these two MDBT patterns reflect a lateral change in La Luna lithology [12]; nonetheless, other explanations such as different biodegradation pathways (e.g., [16]) or selective water washing cannot be totally ruled out [11].

4.6. Geochemical Correlations

A multivariate clustering analysis was carried out based on 10 source-related biological marker parameters (24/23T, Ts/Tm, Pr/Ph, 26/25T, 29/30H, 31R/30H, %27ST, DBT/P, %29ST, and diasterane ratio), following the Ward's algorithm [71]. The Euclidean distance was used to measure divergence since the variance between clusters is maximized while the variance between members of the same cluster is minimized [72]. The resulting dendrogram plot is shown in Figure 9. A single genetic oil type is corroborated by the agglomerative cluster analysis using the proximity procedure, but samples can be grouped into two populations: TJ-872, TJ-1323, and the three oils from the Misoa B7 reservoir on one hand and the remaining samples on the other.

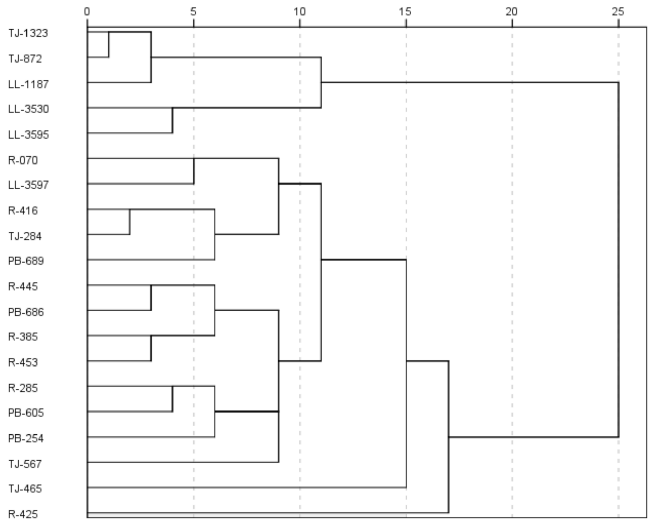

Figure 9. Dendrogram showing the clustering of sampled crude oils.

Classical biomarker distributions (e.g., steranes and triterpanes) and carbon isotope data from the oil samples have been compared to previously reported data from La Luna rock extracts in the eastern edge of Lake Maracaibo [1,15]. Mixed sampled oils correlate well with the marine organic material of the La Luna source rocks. Combination of all data suggests that the mixed oils under study comprise a pre-existing paleobiodegraded petroleum charge, which originated from a first carbonate organic facies of the La Luna Formation, while a fresh post-Oligocene charge sourced from a second more argillaceous and terrigenously derived source facies of the same Upper Cretaceous unit deposited under slightly less oxygen-depleted conditions [12,14]. In this context, the portion of the distinct petroleum charges could explain the differences between the two oil populations and among samples within each of the populations. Such variations are consistent with the different values of the quotient 25-norhopane/30-norhopane [21] for the samples from the Misoa B7 reservoir (<0.15) and those from the Icotea, La Rosa, and Lagunillas intervals (0.2–0.3).

Quantitative extended diamondoid analysis may be used for oil-source rock and oil–oil correlations because almost all source rock extracts and oils contain higher diamondoids, despite thermal maturity or microbial degradation (e.g., [39,73]). QEDA fingerprints from eight extended diamondoids [42] and triamantane were examined in two representative oil samples (Figure 10). TJ-1323 and R-706 oils were clearly differentiated by QEDA. As shown in Figure 10, the main difference between the QEDA fingerprints of both oil samples occurs in the relationship between P4 and H1 (it drops off for the R-706 oil, but H1 is more abundant than P4 in TJ-1323). However, in general, R-706 showed starkly higher relative concentrations of higher polymantanes than TJ-1323, which agrees with the notion that terrigenously derived sources yield lower quantities of diamondoids than marine facies at similar maturation levels [74].

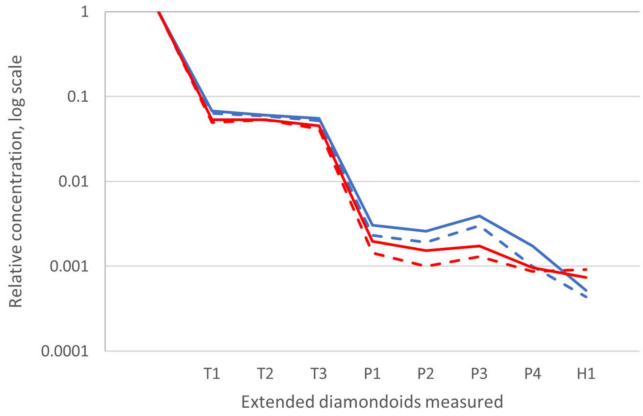

Figure 10. QEDA fingerprints corresponding to TJ-1323 (in red color) and R-706 (in blue color) oils (indicated by continuous lines), and respective hydrous pyrolysates originating from asphaltenic fraction (dash lines). Note: quantities of higher diamondoids are relative to that of triamantane, which is set at one [42].

Comparison of QEDA fingerprints between TJ-1323 and R-706 (saturates) and the respective asphaltene hydrous pyrolysates denoted variances between fingerprints for saturated hydrocarbons of each selected oil sample and its corresponding asphaltene hydrous pyrolysate (Figure 10), indicating that both representative oils consist of mixtures of the almost purely marine carbonate-sourced and more siliciclastic-sourced La Luna oil-types in distinct proportions.

5. Conclusions

The oils analyzed from two fields in the Bolivar Coastal Complex were generated from the same source facies (Upper Cretaceous marine La Luna source rocks deposited in low-oxygen settings), but they are the result of mixing two different petroleum charges, which have been subjected to distinct alteration processes: a biodegraded oil charge during Eocene-Oligocene times and a more mature refreshing during Miocene-Recent times. Biological marker data suggest that the first charge sourced from the La Luna "limestone-rich" facies, while the second pulse originated from the more terrigenously derived "shale-rich" facies of the same Upper Cretaceous formation deposited under slightly less oxygen-depleted conditions. Among our set of oils belonging to the same genetic type, two populations of samples are identified, reflecting different mixing proportions of such organic facies.

Abnormal biodegradation patterns observed in oil samples would be likely the result of adding an unaltered oil charge to a previously degraded hydrocarbon liquid. Variance in the PM levels of alteration within the sampled oils would be explicated by factors such as microbial associations and/or reservoir temperature. Variation in the extent of biodegradation suggests that only the Tía Juana Lago field can produce oil from the deepest reservoirs (Misoa B6/B7) by primary recovery, in contrast with the Cabimas area producing from shallower reservoirs. Lastly, almost identical UMN2 values in the mixed oil samples describe only the extent of alteration of the paleobiodegraded phase.

Author Contributions: Conceptualization, G.M., M.E. and B.G.; methodology, G.M. and M.E.; software, P.M., C.B. and A.P.; validation, E.R., A.B.-S. and A.P.; investigation, G.M., M.E., B.G.; data curation, G.M., B.G.; writing—original draft preparation, M.E., G.M.; writing—review and editing, C.B., P.M., E.R.; visualization, C.B. and P.M.; supervision, G.M., A.P. and A.B.-S.; funding acquisition, G.M. and E.R. All authors have read and agreed to the published version of the manuscript.

Funding: Plan for Research (2019) of the Scientific and Humanistic Development Council of the Central University of Venezuela.

Conflicts of Interest: The authors declare no conflict of interest.

Appendix A

Table A1. Main biomarkers observed in the fragmentograms.

1 C_{21}-tricyclopolyprenane	29 17α(H), 21β(H)-29-Bishomohopane 22R
2 C_{23}-tricyclopolyprenane	30 17α(H), 21β(H)-29-Trishomohopane 22S
3 C_{24}-tricyclopolyprenane	31 17α(H), 21β(H)-29-Trishomohopane 22R
4 C_{25}-tricyclopolyprenane 17R + 17S	32 17α(H), 21β(H)-29-Tetrahomohopane 22S
5 C_{26}-tricyclopolyprenane 17R	33 17α(H),21β(H)-29-Tetrahomohopane 22R
6 C_{24}-tricyclopolyprenane	34 17α(H),21β(H)-29-Pentahomohopane 22S
7 C_{26}-tricyclopolyprenane 17S	35 17α(H),21β(H)-29-Pentahomohopane 22R
8 C_{28}-tricyclopolyprenane 17R	36 13β(H),17α(H)-Diacholestane 20S
9 C_{28}-tricyclopolyprenane 17S	37 13β(H),17α(H)-Diacholestane 20R
10 C_{29}-tricyclopolyprenane 17R	38 5α(H),14α(H),17α(H)-Cholestane 20S *
11 C_{29}-tricyclopolyprenane 17S	39 5α(H),14β(H),17β(H)-Cholestane 20R *
12 18α(H)-22,29,30-Trisnorneohopane	40 5α(H),14 β(H),17β(H)-Cholestane 20S
13 C_{30}-Tricyclic terpane 17R	41 5α(H),14α(H),17α(H)-Cholestane 20R
14 17α(H)-22,29,30-Trisnorhopane	42 5α(H),14α(H),17α(H)-Ergostane 20S
15 C_{30}-Tricyclic terpane 17S	43 5α(H),14β(H),17β(H)-Ergostane 20R *
16 18α(H)-24,28-Bisnoroleanane	44 5α(H),14β(H),17β(H)-Ergostane 20S
17 17α(H),21β(H)-30-Norhopane	45 5α(H),14α(H),17α(H)-Ergostane 20R
18 18α(H)-30-Norneohopane	46 5α(H),14α(H),17α(H)-Stigmastane 20S
19 18α(H)-28-Noroleanane	47 5α(H),14β(H),17β(H)-Stigmastane 20R
20 17β(H),21α(H)-30-Normoretane	48 5α(H),14β(H),17β(H)-Stigmastane 20S
21 18α(H)-Oleanane	49 5α(H),14α(H),17α(H)-Stigmastane 20R
22 17α(H),21β(H)-Hopane	50 20-triaromatic steroid
23 17β(H),21α(H)-Moretane	51 21-triaromatic steroid
24 17α(H),21β(H)-29-Homohopane 22S	52 26-triaromatic steroid 20S
25 17α(H),21β(H)-29-Homohopane 22R	53 26 (20R) + 27 (20S)-triaromatic steroid *
26 Gammacerane	54 28-triaromatic steroid 20S
27 17β(H),21α(H)-29-Homomoretane 22S + 22R	55 27-triaromatic steroid 20R
28 17α(H),21β(H)-29-Bishomohopane 22S	56 28-triaromatic steroid 20R

* Peak coelution.

References

1. Talukdar, S.; Gallango, O.; Chin-A-Lien, M. Generation and migration of hydrocarbons in the Maracaibo basin, Venezuela: An integrated basin study. *Org. Geochem.* **1986**, *10*, 261–279. [CrossRef]
2. Tocco, R.; Gallango, O.; Parnaud, F. Geochemical modelling of the principal source rocks of the Barinas and Maracaibo basins, western Venezuela. *Bull. Venez. Soc. Geol.* **1997**, *22*, 17–28.
3. Talukdar, S.; Marcano, F. Petroleum system of the Maracaibo Basin, Venezuela. In *The Petroleum System—For Source to Trap*; Magoon, L.B., Dow, W.G., Eds.; AAPG Memoir: Tulsa, OK, USA, 1994; Volume 60, pp. 463–481.
4. Bockmeulen, H.; Barker, C.; Dickey, P.A. Geology and Geochemistry of Crude Oils, Bolivar Coastal Fields, Venezuela. *AAPG Bull.* **1983**, *67*, 242–270.
5. Villalobos, C.K. Geoquímica de los crudos del Miembro B6 (Eoceno), campo Tía Juana Lago, Cuenca del Lago de Maracaibo. Master's Thesis, University of Zulia, Maracaibo, Venezuela, 2012.
6. Guerrero, B.R. Revisión del proceso de biodegradación del petróleo presente en las formaciones Lagunillas inferior, La Rosa e Icotea del campo Cabimas. Master's Thesis, University of Zulia, Maracaibo, Venezuela, 2016.
7. Rey, O.; Simo, J.; Lorente, M. A record of long- and short-term environmental and climatic change during OAE3: La Luna Formation, Late Cretaceous (Santonian–early Campanian), Venezuela. *Sediment. Geol.* **2004**, *170*, 85–105. [CrossRef]
8. Lugo, J.; Mann, P. Jurassic-Eocene Tectonic evolution of Maracaibo basin, Venezuela. *AAPG Mem.* **1995**, *62*, 699–725.
9. Parnaud, F.; Gou, Y.; Pascual, J.C.; Capello, M.A.; Truskowski, I.; Passalaqua, H. Stratigraphic synthesis of Western Venezuela. In *Petroleum Basins of South America*; Tankar, A.J., Suárez-Soruco, R., Welsink, H.J., Eds.; AAPG Memoir: Tulsa, OK, USA, 1995; Volume 62, pp. 681–698.
10. Erlich, R.N.; Villamil, T.; Keen-Dumas, J. Controls on the deposition of Upper Cretaceous organic carbon-rich rocks from Costa Rica to Surinam. In *The Circum-Gulf of Mexico and the Caribbean: Hydrocarbon Habitats, Basin Formation, and Plate Tectonics*; Bartolini, C., Buffler, R., Blickwede, J., Eds.; AAPG Memoir: Tulsa, OK, USA, 2003; Volume 79, pp. 1–45.
11. Galarraga, F.; Urbani, F.; Escobar, M.; Márquez, G.; Martínez, M.; Tocco, R. Main factors controlling the compositional variability of seepage oils from Trujillo State, Western Venezuela. *J. Pet. Geol.* **2010**, *33*, 255–268. [CrossRef]
12. Erlich, R.N.; Macsotay, O.; Nederbragt, A.J.; Lorente, M.A. Palaeoecology, palaeogeography and depositional environments of Upper Cretaceous rocks of western Venezuela. *Palaeogeogr. Palaeoclimatol. Palaeoecol.* **1999**, *153*, 203–238. [CrossRef]
13. Sweeney, J.; Talukdar, S.; Burnham, A.; Vallejos, C. Pyrolysis kinetics applied to prediction of oil generation in the Maracaibo Basin, Venezuela. *Org. Geochem.* **1990**, *16*, 189–196. [CrossRef]
14. Márquez, G.; Escobar, M.; Lorenzo, E.; Duno, L.; Esquinas, N.; Gallego, J.R. Intra- and inter- field compositional changes of oils from the Misoa B4 reservoir in the Ceuta Southeast Area (Lake Maracaibo, Venezuela). *Fuel* **2016**, *167*, 118–134. [CrossRef]
15. Márquez, G.; Escobar, M.; Esquinas, N.; Duno, L.; Martín-Martín, J.D.; Permanyer, A. Characterization of tar-like material and producible oil in Misoa C2 and C3 reservoir sands of the Area 2 South (Ceuta field, Venezuela). *Mar. Pet. Geol.* **2017**, *82*, 118–133. [CrossRef]
16. Head, I.M.; Jones, D.M.; Larter, S.R. Biological activity in the deep subsurface and the origin of heavy oil. *Nature* **2003**, *426*, 344–352. [CrossRef] [PubMed]
17. Wardlaw, G.D.; Nelson, R.K.; Reddy, C.M.; Valentine, D.L. Biodegradation preference for isomers of alkylated naphthalenes and benzothiophenes in marine sediment contaminated with crude oil. *Org. Geochem.* **2011**, *42*, 630–639. [CrossRef]
18. Larter, S.R.; Wilhelms, A.; Head, I.M.; Koopmans, M.; Aplin, A.; di Primio, R.; Erdmann, M.; Telnaes, N. The controls on the composition of biodegraded oils in the deep subsurface—Part 1: Biodegradation rates in petroleum reservoirs. *Org. Geochem.* **2003**, *34*, 601–613. [CrossRef]
19. Adams, J.J.; Riediger, C.; Fowler, M.; Larter, S.R. Thermal controls on biodegradation around the Peace River tar sands: Paleo-pasteurization to the west. *J. Geochem. Expor.* **2006**, *89*, 1–4. [CrossRef]

20. Larter, S.R.; Gates, I.; Adams, J.; Bennet, B.; Huang, H.; Koksalan, T.; Fustic, M. Reservoir fluid characterization of tar sand and heavy oil reservoirs-impact of fluid heterogeneity on production characteristics. In Proceedings of the AAPG Annual Convention -Perfecting the Search- Delivering on Promises, Houston, TX, USA, 9–12 April 2006.
21. Volkman, J.K.; Robert, A.; Robert, I.K.; Woodhouse, C.W. Demethylated hopanes in crude oils and their applications in petroleum geochemistry. *Geochim. Cosmochim. Acta* **1983**, *47*, 785–794. [CrossRef]
22. Peters, K.E.; Moldowan, J. *The Biomarker Guide: Interpreting Molecular Fossils in Petroleum and Ancient Sediments*; Prentice Hall: Englewood Cliffs, NJ, USA; New York, NY, USA, 1993; p. 363.
23. Wenger, L.M.; Davis, C.L.; Isaksen, G.J. Multiple controls on petroleum biodegradation and impact on oil quality. *SPE Reserv. Eval. Eng.* **2002**, *5*, 375–383. [CrossRef]
24. Larter, S.R.; Huang, H.; Adams, J.; Bennet, B.; Snowdon, L.R. A practical biodegradation scale for use in reservoir geochemical studies of biodegraded oils. *Org. Geochem.* **2012**, *45*, 66–76. [CrossRef]
25. Macellari, C.E. Cretaceous paleogeography and depositional cycles of western South America. *J. S. Am. Earth Sci.* **1988**, *1*, 373–418. [CrossRef]
26. Mann, P. Caribbean sedimentary basins: Classification and tectonic setting from Jurassic to present. Caribbean Basins. *Sediment. Basins World* **1999**, *4*, 3–31.
27. Castillo, M.; Mann, P. Cretaceous to Holocene structural stratigraphic development in south Lake Maracaibo, Venezuela, inferred from well and three-dimensional seismic data. *AAPG Bull.* **2006**, *90*, 529–565. [CrossRef]
28. Escalona, A.; Mann, P. An overview of the petroleum system of Maracaibo Basin. *AAPG Bull.* **2006**, *90*, 653–674. [CrossRef]
29. Mann, P.; Escalona, A.; Castillo, M. Regional geologic and tectonic setting of the Maracaibo supergiant basin, Western, Venezuela. *AAPG Bull.* **2006**, *90*, 445–477. [CrossRef]
30. Wills, V.C. Modelo estático en 3D del Mioceno del área Cabimas, Campo Costanero Bolivar, Cuenca de Maracaibo. Master's Thesis, Central University of Venezuela, Caracas, Venezuela, 2009.
31. Márquez, L.C. Caracterización del campo Ambrosio para planes de desarrollo gasífero. Bachelor's Thesis, Central University of Venezuela, Caracas, Venezuela, 2004.
32. Walton, W.M. Contributions of the AVGMP Maracaibo Basin Eocene Nomenclature Comittee: The informal units of the subsurface Eocene. Asociación Venezolana de Geología, Minería y Petróleo. *Boletín Inf.* **1967**, *10*, 21–30.
33. Rodríguez, I.; Navarro, A.; Ghosh, S. Nueva Frontera Exploratoria en la Cuenca Petrolífera del Lago de Maracaibo: Zulia Oriental, Venezuela Occidental. In Proceedings of the Memorias VI Simposio Bolivariano de Exploración de Cuencas Subandinas, Cartagena, Colombia; Asociación Colombiana de Geólogos y Geofísicos del Petróleo, Bogota, Colombia, 14–17 September 1997; pp. 565–581.
34. Urbina, E.R. Determinación de registros psudo-sónicos a partir de registros de resistividad en los campos Barúa, Motatán y Tomopoto. Bachelor's Thesis, Central University of Venezuela, Caracas, Venezuela, 2001.
35. *ASTM Standard Test Method for API Gravity of Crude Petroleum and Petroleum Products (Hydrometer Method)*; ASTM International: West Conshohocken, PA, USA, 2006.
36. *ASTM Standard Test Method for Sulfur in Petroleum and Petroleum Products by Energy Dispersive X-ray Fluorescence Spectrometry*; ASTM International: West Conshohocken, PA, USA, 2010.
37. Speight, J.G. *The Chemistry and Technology of Petroleum*; CRC Press: Boca Raton, FL, USA, 2007.
38. De la Cruz, C.; Márquez, N.; Escobar, M.; Segovia, S. An improved chromatographic method for the separation of saturated hydrocarbons, aromatic hydrocarbons, resins and asphaltenes from heavy crude oils. In Proceedings of the 213th American Chemical Society National Meeting, San Francisco, CA, USA, 13–17 April 1997; pp. 416–418.
39. Dahl, J.E.; Moldowan, J.M.; Peters, K.E.; Claypool, G.E.; Rooney, M.A.; Michael, G.E.; Mello, M.R.; Kohnen, M.L. Diamondoid hydrocarbons as indicators of natural oil cracking. *Nature* **1999**, *399*, 54–57. [CrossRef]
40. Pytlak, L.; Kowalski, A.; Gross, D.; Sachsenhofer, R.F. Composition of diamondoids in oil samples from the alpine foreland basin, austria: Potential as indices of source rock facies, maturity and biodegradation. *J. Pet. Geol.* **2017**, *40*, 153–171. [CrossRef]
41. Summons, R.E.; Hope, J.M.; Swart, R.; Walter, M.R. Origin of Nama Basin bitumen seeps: Petroleum derived from a Permian lacustrine source rock traversing southwestern Gondwana. *Org. Geochem.* **2008**, *39*, 589–608. [CrossRef]

42. Moldowan, J.M.; Dahl, J.; Zinniker, D.; Barbanti, S.M. Underutilized advanced geochemical technologies for oil and gas exploration and production-1. *J. Pet. Sci. Eng.* **2015**, *126*, 87–96. [CrossRef]
43. Tissot, B.P.; Welte, D.H. *Petroleum Formation and Occurrence*; Springer: New York, NY, USA, 1984; p. 699.
44. Hakimi, M.H.; Abdullaha, W.H.; Shalabya, M.R. Organic geochemical characteristics of crude oils from the Masila Basin, eastern Yemen. *Org. Geochem.* **2011**, *42*, 465–476. [CrossRef]
45. Peters, K.E.; Walters, C.; Moldowan, J. *The Biomarker Guide: Biomarkers and Isotopes in Petroleum Systems and Earth History*; Cambridge University Press: Cambridge, UK, 2005; p. 1132.
46. Sofer, Z. Stable Carbon Isotope composition of crude oils: Application to source depositional environments and petroleum alteration. *AAPG Bull.* **1984**, *68*, 31–49.
47. Meckenstock, R.U.; Morasch, B.; Warthmann, R.; Schink, B.; Annweiler, E.; Michaelis, W.; Richnow, H.H. 13C/12C isotope fractionation of aromatic hydrocarbons during microbial degradation. *Environ. Microbiol.* **1999**, *1*, 409–414. [CrossRef]
48. Milner, C.D.W.; Rogers, M.A.; Evans, C.R. Petroleum transformations in reservoirs. *J. Geochem. Explor.* **1977**, *7*, 101–153. [CrossRef]
49. Bennet, B.; Fustic, M.; Farrimond, P.; Huang, H.; Larter, S.R. 25-Norhopanes: Formation during biodegradation of petroleum in the subsurface. *Org. Geochem.* **2006**, *37*, 787–797. [CrossRef]
50. Hunt, J.M. *Petroleum Geochemistry and Geology*; Freeman and Company: San Francisco, CA, USA, 1996; p. 617.
51. Philp, R.P. *Fossil Fuel Biomarkers: Applications and Spectra*; Elsevier Science Publishers: New York, NY, USA, 1985; p. 294.
52. Liao, Z.; Geng, A.; Gracia, A.; Creux, P.; Chrostowska, Y.; Zhang, Y. Saturated hydrocarbons occluded inside asphaltene structures and their geochemical significance, as exemplified by two Venezuelan oils. *Org. Geochem.* **2006**, *37*, 291–303. [CrossRef]
53. Volkman, J.K.; Alexander, R.; Kagi, R.I.; Rowland, S.J.; Sheppard, P.N. Biodegradation of aromatic hydrocarbons in crude oils from the Barrow Sub-basin of Western Australia. *Org. Geochem.* **1984**, *6*, 619–632. [CrossRef]
54. Huang, H.P.; Bowler, B.F.J.; Oldenburg, T.B.P.; Larter, S.R. The effect of biodegradation on polycyclic aromatic hydrocarbons in reservoired oils from the Liaohe basin, NE China. *Org. Geochem.* **2004**, *35*, 1619–1634. [CrossRef]
55. Sánchez, C.; Permanyer, A. Origin and alteration of oils and oil seeps from the Sinú-San Jacinto Basin, Colombia. *Org. Geochem.* **2006**, *37*, 1831–1845. [CrossRef]
56. Escobar, M.; Márquez, G.; Inciarte, S.; Rojas, J.; Esteves, I.; Malandrino, G. The organic geochemistry of oil seeps from the Sierra de Perijá eastern foothills, Lake Maracaibo Basin, Venezuela. *Org. Geochem.* **2011**, *42*, 727–738. [CrossRef]
57. Mackenzie, A.S. Applications of biological markers in petroleum geochemistry. In *Advances in Petrological Geochemistry*; Brooks, S.J., Welte, D., Eds.; Academic Press: London, UK, 1984; pp. 115–214.
58. Radke, M.; Welte, D.H. The methylphenantrene index (MPI): A maturity parameter based on aromatic hydrocarbons. In *Advances in Organic Geochemistry*; Bjoroy, M., Albrecht, C., Cornford, C., de Groot, K., Eglinton, G., Galimov, E., Leythaeuser, D., Pelet, R., Rullkötter, J., Speers, G., Eds.; John Wiley and Sons: New York, NY, USA, 1983; pp. 504–512.
59. Radke, M.; Leythaeuser, D.; Teichmüller, M. Relationship between rank and composition of aromatic hydrocarbons from coals of different origin. *Org. Geochem.* **1984**, *6*, 423–430. [CrossRef]
60. Cassani, F.; Gallango, O.; Talukdar, S.; Vallejos, C.; Ehrmann, U. Methylphenanthrene maturity index of marine source rock extracts and crude oils from the Maracaibo Basin. *Org. Geochem.* **1988**, *13*, 73–80. [CrossRef]
61. Bennett, B.; Larter, S. Biodegradation scales: Applications and limitations. *Org. Geochem.* **2008**, *39*, 1222–1228. [CrossRef]
62. Radke, M.; Welte, D.H.; Willsch, H. Geochemical study on a well in the Western Canada Basin: Relation of the aromatic distribution pattern to maturity of organic matter. *Geochim. Cosmochim. Acta* **1982**, *46*, 1–10. [CrossRef]
63. Radke, M.; Welte, D.H.; Willsch, H. Maturity parameters based on aromatic hydrocarbons: Influence of the organic matter type. *Org. Geochem.* **1986**, *10*, 51–63. [CrossRef]
64. Kotarba, M.J.; Clayton, J.L. A stable carbon isotope and biological marker study of Polish bituminous coals and carbonaceous shales. *Int. J. Coal. Geol.* **2003**, *55*, 73–94. [CrossRef]

65. Hughes, W.B.; Holba, A.G.; Dzou, L.I.P. The ratios of dibenzothiophene to phenanthrene and pristane to phytane as indicators of depositional environment and lithology of petroleum source rocks. *Geochim. Cosmochim. Acta* **1995**, *59*, 3581–3598. [CrossRef]
66. Van Graas, G.W. Biomarker maturity parameters for high maturities: Calibration of the working range up to the oil/condensate threshold. *Org. Geochem.* **1990**, *16*, 1025–1032. [CrossRef]
67. Palacas, J.G. Carbonate rocks as sources of petroleum: Geological and chemical characteristics and oil-source correlations. *World Pet. Congr.* **1983**, *11*, 31–33.
68. Seifert, W.K.; Moldowan, J.M. Palaeoreconstruction by biological markers. *Geochim. Cosmochim. Acta* **1981**, *45*, 783–794. [CrossRef]
69. Rullkötter, J.; Spiro, B.; Nissenbaum, A. Biological marker characteristics of oils and asphalts from carbonate source rocks in a rapidly subsiding graben, Dead Sea, Israel. *Geochim. Cosmochim. Acta* **1985**, *49*, 1357–1370. [CrossRef]
70. Grantham, P.J.; Wakefield, L.L. Variations in the sterane carbon number distributions of marine source rocks derived crude oils through geological time. *Org. Geochem.* **1988**, *12*, 61–73. [CrossRef]
71. Gallego, J.R.; Ortiz, J.E.; Sierra, C.; Torres, T.; Llamas, J.F. Multivariate study of trace element distribution in the geological record of Roñanzas peat bog (Asturias, North Spain): Paleoenvironmental evolution and human activities over the last 8000 ca yr BP. *Sci. Total Environ.* **2013**, *454/455*, 16–29. [CrossRef]
72. Everitt, B.S. Cluster Analysis. In *Multivariate Statistics*; Edward, A., Ed.; Oxford University Press: London, UK, 1993; pp. 42–50.
73. Grice, K.; Alexander, R.; Kagi, R.I. Diamondoid hydrocarbon ratios as indicators of biodegradation in Australian crude oils. *Org. Geochem.* **2000**, *31*, 67–73. [CrossRef]
74. Jiang, W.M.; Li, Y.; Xiong, Y.Q. The effect of organic matter type on formation and evolution of diamondoids. *Mar. Pet. Geol.* **2018**, *89*, 714–720. [CrossRef]